

THE EXTENT OF MAGNETIC FIELDS AROUND GALAXIES OUT TO $Z \sim 1$

M.L. BERNET^{2,3}, F. MINIATTI², S. J. LILLY²

Submitted

ABSTRACT

Radio quasar sightlines with strong MgII absorption lines display statistically enhanced Faraday Rotation Measures (RM) indicating the presence of additional magneto-active plasma with respect to sightlines free of such absorption. In this letter, we use multi-color optical imaging to identify the likely galaxies hosting the magneto-active plasma, and to constrain the location of the latter with respect to the putative parent halo. We find that all of the sightlines with high |RM| pass within 50 kpc of a galaxy and that the |RM| distribution for low impact parameters, $D < 50$ kpc, is significantly different than for larger impact parameters. In addition, we find a decrease in the ratio of the polarization at 21 cm and 1.5 cm, $p_{21}/p_{1.5}$, towards lower D . These two effects are most likely related, strengthen the association of excess |RM| with intervening galaxies, and suggest that intervening galaxies operate as inhomogeneous Faraday screens. These results are difficult to reconcile with only a disk model for the magnetic field but are consistent with highly magnetized winds associated with MgII systems. We infer strong magnetic fields of a few tens of μG , consistent with values required by the lack of evolution of the FIR-radio correlation at high redshifts. Finally, these findings lends support to the idea that the small scale helicity bottleneck of α - Ω galactic dynamos can be significantly alleviated via galactic winds.

Subject headings: galaxies: high-redshift — galaxies: magnetic fields — quasars: absorption lines — galaxies: evolution

1. INTRODUCTION

The origin and evolution of magnetic fields in galaxies over cosmic time is observationally still largely unconstrained. For normal galaxies at significant look-back times, statistical studies of the Faraday Rotation effect on luminous polarized background sources provide the most effective way to probe magnetic fields. In Bernet et al. (2008, 2010) we presented evidence that quasars with strong intervening MgII absorption lines in their optical spectra (with equivalent width, $EW_0 > 0.3\text{\AA}$) have a significantly broader distribution of Rotation Measure (RM) than those without. Bernet et al. (2010) showed that this was unlikely to be due to any indirect correlation with the quasar redshift, since the effect was not present for sightlines with weaker MgII absorption. Since strong MgII absorption is known to be generally associated with the halos of normal galaxies, the simplest interpretation was that $\sim 10 \mu\text{G}$ large scale magnetic fields exist in or around galaxies out to $z \sim 1.3$ (Bernet et al. 2008).

In this Letter we study the radio properties of background quasars at different impact parameters from the MgII host galaxies responsible for the enhanced RM. A similar approach has been used to study individual nearby galaxies, e.g. M31 (Han et al. 1998), the LMC (Gaensler et al. 2005) and the SMC (Mao et al. 2008), which have numerous polarized background sources

available. For distant galaxies this is not viable and a statistical approach is necessary.

Our study reveals that strong magnetic fields are present around galaxies out to large impact parameters of order 50 kpc. Applying recent results from the study of MgII systems (Bordoloi et al. 2011, 2012), this suggests that the ubiquitous winds in high redshift galaxies (Weiner et al. 2009; Bordoloi et al. 2011; Rubin et al. 2010) are highly magnetized. Furthermore, this finding provides support to the idea that magnetized outflows help removing small scale helicity from galactic disks (Shukurov et al. 2006), preventing the quenching of α - Ω dynamo mechanism (Vainshtein & Cattaneo 1992), thought to generate the large scale magnetic fields in galactic disks (Brandenburg & Subramanian 2005).

Where required, we assume a concordance cosmology with $h = 0.71$, $\Omega_M = 0.27$ and $\Omega_\Lambda = 0.73$.

2. OBSERVATIONS AND DATA REDUCTION

We obtained images of the fields of 28 radio quasars with strong MgII absorption lines selected from the sample of Bernet et al. (2008).

Images were taken in three bands with the EFOSC2 instrument at the NTT in P82 from 30.10.08 - 02.11.08 and in P85 from 15.03.10 - 18.03.10. The quasar fields with absorbers in the redshift range 0.4 - 0.8 were observed with g, r, i filters and those with absorbers in the range 0.8 - 1.4 with the r, i, z filters. These filters were chosen in order to straddle the 4000 \AA break at the redshifts of the absorber. The total exposure times in each filter varied between 600-6000s depending on the redshift of the absorbers. We aimed to detect galaxies down to $0.1 L^* \text{ }^3$ at the absorber redshift. To facilitate PSF for

³ L^* is the characteristic galaxy luminosity of the Schechter function where the power law cuts off.

¹ Based on observations made with the ESO Telescopes at the La Silla Observatories under programme 082.A-0917 and 085.A-0417. mbernet@swin.edu.au, fm@phys.ethz.ch, simon.lilly@phys.ethz.ch

² Physics Department, ETH Zurich, Wolfgang-Pauli-Strasse 27, CH-8093 Zurich, Switzerland

³ Centre for Astrophysics and Supercomputing, Swinburne University of Technology, Hawthorn, Melbourne, Victoria 3122, Australia

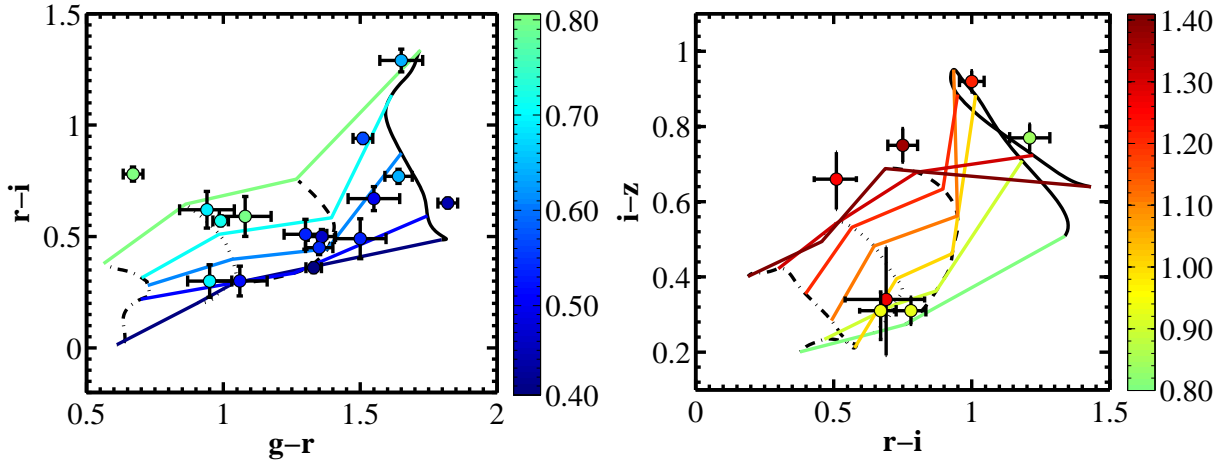


FIG. 1.— $g-r$ vs. $r-i$ and $r-i$ vs. $i-z$ plot of identified host galaxies of the MgII absorption systems in the redshift range $0.4 < z_{MgII} < 0.8$ and $0.8 < z_{MgII} < 1.4$, respectively. The loci of an elliptical, Sbc, Scd and irregular galaxy are shown as solid, dashed, dotted and dashed-dotted lines. The color code indicates the photometric redshift of the galaxies.

subtraction of the quasar, the camera was used in the 1x1 binning mode giving a pixel scale of 0.12 arcsec per pixel.

In order to identify the MgII host galaxies, we place the galaxies in the quasar field on a color-color diagram and compare them with the theoretical loci of galaxies of different types computed from spectral energy distributions from Coleman et al. (1980) as a function of redshift. The photometry of the galaxies was done using SExtractor (Bertin & Arnouts 1996). The flux was measured in each filter using circular apertures with diameter of typically 30 pixels, corresponding to 3.6 arcsecs. This was reduced when necessary to avoid contamination by neighbouring objects.

To identify the host galaxy we proceed as follows:

- i) Measure the $(r-i)$ and $(g-r)$ or $(i-z)$ colors of all the galaxies within 120 kpc of the quasar at the redshift of the absorber. In cases where there was no detection of a galaxy in one of the bands, upper limits were calculated for that band.
- ii) All galaxies that have colors in the color-color diagram consistent with the locus of SED-types at the redshift of the MgII system (see Fig. 1), are considered as candidate host galaxies. When in regions of color-color space there is a degeneracy between SED-type and redshift a morphological classification was done in order to separate these two quantities.
- iii) For objects very close to the quasar, within $\sim 2''$, it was not possible to do accurate photometry of the galaxies. We assume that all three objects within $\sim 2''$ are the host. (See Chen et al. (2010)).
- iv) In cases where there were two candidate host galaxies, both with consistent colors, the closer one to the quasar was selected when the impact parameter differed by more than a factor two. For cases where they differed by less than a factor two the impact parameters were averaged (PKS2204-54, 4C+19.34, 4C+13.46, PKS0506-61, PKS0038-020).

The properties of the identified host galaxies are given in Table 1. While there is inevitably a certain arbitrariness to the identification of the host galaxies, we emphasize that this process was carried out blind with respect to the RM values of the quasars in order to preserve the statistical integrity of the analysis. For the quasar field 4C+06.41 (Lanzetta et al. 1995) and 4C+19.44 (Kacprzak et al. 2008) spectroscopic redshifts of galaxies are available and those agree with our choice of host galaxies.

The RMs in this work are selected from the sample of Kronberg et al. (2008) at Galactic latitudes $|b| > 30^\circ$. At least three polarization angles, typically measured at wavelengths around 6 cm, were used for the RM determination (for more details see Bernet et al. 2012).

3. RESULTS

3.1. $|\text{RM}|$ vs. impact parameters

In Fig. 2 we plot the observed $|\text{RM}|$, uncorrected for Galactic foreground, for the 28 sightlines containing strong MgII absorption systems, against the impact parameter D to the identified host galaxies. Filled circles show sightlines with a single MgII system and a uniquely identified intervening galaxy. Open circles correspond to the case of two candidate host galaxies plotted at average impact parameter (see (iv) above). Crossed symbols correspond to the case in which a foreground galaxy lies closer to the line of sight than the MgII host galaxy and which is therefore likely to have contaminated the RM value. Open squares indicate quasars sightlines with two strong MgII systems. Full details about each sightline are provided in Table 1.

Fig. 2 shows that the $|\text{RM}|$ increases significantly towards sightlines with smaller impact parameter. All $|\text{RM}|$ values $> 50 \text{ rad m}^{-2}$ are at $D < 50 \text{ kpc}$. At significantly larger impact parameter, $> 60 \text{ kpc}$, the RM is mostly given by the Milky Way contribution and observational error (horizontal dash line), which amount to $\sim 20 \text{ rad m}^{-2}$ (Bernet et al. 2008). This is similar to the 68% percentile spread of the $|\text{RM}|$ for quasars without MgII absorption, i.e. to $|\text{RM}|_{68} \sim 25 \text{ rad m}^{-2}$ (Bernet et al. 2010). Note that Galactic

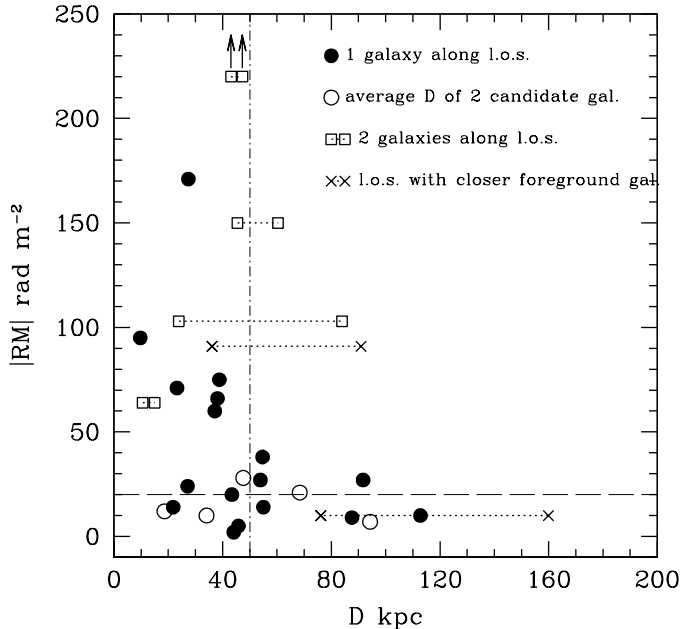


FIG. 2.— Observed $|RM|$ vs. impact parameters D of the quasar sightlines to the host galaxies of the MgII absorption systems. Solid circles show l.o.s. with one MgII system and with a unique association of the galaxy which produces the RM. Open circles show l.o.s. with one MgII system but with two possible host galaxies and where the impact parameters differ by less than a factor two (shown at average D). The cross symbol corresponds to a l.o.s. where next to the galaxy at z_{MgII} a foreground galaxy was detected at smaller impact parameter and at $z \neq z_{MgII}$. The horizontal dashed line indicates the 20 rad m^{-2} level below which Galactic RM dominates. For illustration purposes the $|RM|$ value of QSO sightline PKS2326-477 is shown at $|RM| = 220 \text{ rad m}^{-2}$ instead of 360 rad m^{-2} . The typical error on the observed RM is $\sim 3.5 \text{ rad m}^{-2}$ (median).

foreground as, e.g., in Oppermann et al. (2012) does not introduce any trend with impact parameter, while it contributes to our sources a median $|RM| 12.6 \text{ rad m}^{-2}$.

A Pearson¹ test for correlation for the circles in Fig. 2 shows that $|RM|$ and D are anticorrelated with $\rho = -0.43$, corresponding to a chance probability of $p = 4.8\%$. A two-sided Kolmogorov-Smirnov (KS) test for the same data reveals a chance probability that the $|RM|$ distributions below and above 40 kpc are drawn from the same distribution of $p = 2.2\%$.

This analysis corroborates the above result that the RM contribution is negligible for sightlines beyond 60 kpc. We can therefore try and repeat the KS-test including the two sightlines with closer foreground galaxies without MgII absorption (x symbols), and also the four sightlines with two MgII systems (open squares), assuming that only galaxies with $D < 50$ kpc contribute RM. This lowers the above chance probability to $p = 1.5\%$ and 1.9% , if we split the sample at 40 and 50 kpc, respectively.

Using the sightlines with one MgII absorber at $D < 50$ kpc we determine an observed dispersion of RM $\sigma_{obs} \sim 65 \text{ rad m}^{-2}$. The contribution from the intrinsic RM, the Milky Way RM, and the observational error is found from sightlines without absorbers to be $\sim 25 \text{ rad m}^{-2}$. Subtracting in quadrature and multiplying by $(1+z_{MgII})^2$, we obtain a rest frame RM dispersion for the MgII absorbers $\sigma_{MgII} \sim 150 \text{ rad m}^{-2}$.

3.2. Inhomogeneity of the RM screens

In Bernet et al. (2012) we studied the effect of depolarisation due to inhomogeneous Faraday screens in intervening galaxies at redshift z , with RM dispersion σ_{RM} and covering factor f_c . We predicted a wavelength λ dependent effect, $p(\lambda^2)/p_0 = f_c \exp(-2\sigma_{RM}^2(1+z)^{-4}\lambda^4) + (1-f_c)$, where p_0 is the intrinsic polarisation. Since according to Fig. 2 the observed RM dispersion increases for smaller impact parameter, we expect the degree of polarization to follow a similar pattern.

In order to test the depolarization potentially suffered by our sources, we use the ratio $p_{21}/p_{1.5}$, where p_{21} and $p_{1.5}$ are the degrees of polarization at 21 and 1.5 cm, from Taylor et al. (2009) and Condon et al. (1998), and from Jackson et al. (2010) and Murphy et al. (2010), respectively. Since in general the short and long wavelength emission originate from different components of the radio source (i.e. the compact core and the radio lobes), the above ratio is not a “measure” of depolarization. However, due to the wavelength dependence of the depolarization effect, statistically the ratio $p_{21}/p_{1.5}$ will be lower the stronger the depolarizing effect along the line of sight.

In Fig. 3 we plot the ratio $p_{21}/p_{1.5}$ versus the impact parameters D to the galaxies. Solid/open circles indicate if the quasar redshift is > 1.0 or < 1.0 . Due to the low number of quasar fields for which both $p_{21}/p_{1.5}$ and D are available, this plot also includes two sightlines with multiple absorbers, shown as solid squares. For one of them (PKS 1143-245) one galaxy is at 21 kpc and the other at 84 kpc, so it is likely that only the closer one is contributing. For the other (4C-02.55) both galaxies are close in, at 10.6 kpc and 11.8 kpc from the sightline, respectively, so both are likely contributing to the observed RM.

A clear trend is visible in Fig. 3 in the left hand panel, whereby the lower the impact parameter, the lower the value of $p_{21}/p_{1.5}$. A Kendall’s τ test shows that for the overall sample, $p_{21}/p_{1.5}$ and D are correlated with $\tau = 0.30$ and a chance probability of 11.6%. Knowing that quasars with $z_{QSO} < 1.0$ are intrinsically more depolarized than those above this redshift (Bernet et al. 2012) we split the sample according to this redshift. This effectively separates out two objects with low $p_{21}/p_{1.5}$ values at high impact parameters. Repeating now the test for the $z_{QSO} > 1.0$ sample shows that $p_{21}/p_{1.5}$ and D are strongly correlated with $\tau = 0.56$ and a chance probability of only 1.7%. For comparison, the $p_{21}/p_{1.5}$ for sightlines from the whole Bernet et al. (2008) sample that do not have MgII absorption systems and are at $z_{QSO} > 1.0$ are plotted in the right hand panel in Fig. 3.

As in Bernet et al. (2012), a Faraday screen can be modeled as a collection of cells of size l_c , the magnetic field coherence length. The (rest frame) RM dispersion of the cells on a Faraday screen of depth L is then written as:

$$\sigma_{RM} = \sigma_c \sqrt{L/l_c} \propto B n_e l_c \sqrt{L/l_c}, \quad (1)$$

where $\sigma_c \propto B n_e l_c$ is the RM of a single cell. We can now relate σ_{RM} to the (rest-frame) RM dispersion characterizing sightlines through a galactic Faraday screen, σ_{MgII} , by

$$\sigma_{RM} = \sigma_{MgII} \sqrt{N/f_c}, \quad (2)$$

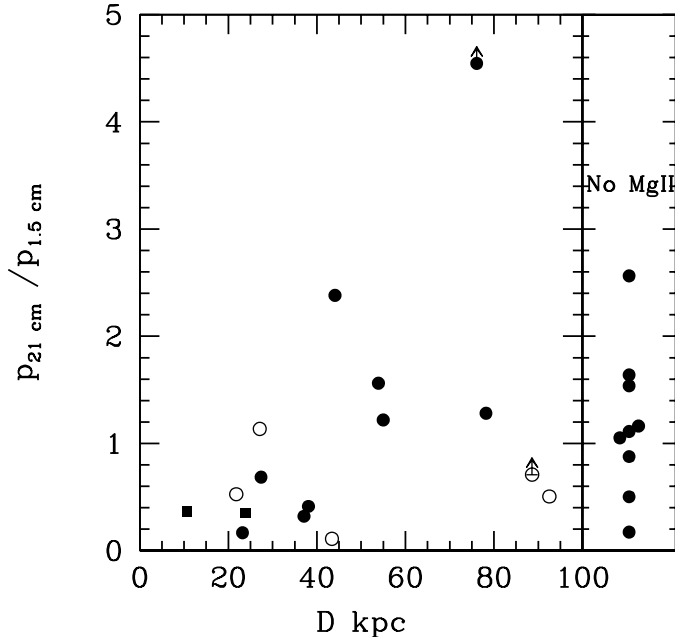


FIG. 3.— Depolarization proxy, $p_{21}/p_{1.5}$, as a function of the intervening galaxies' impact parameter. Solid circles show QSO at $z > 1.0$ and open circles at $z < 1.0$. For the two QSO fields with two intervening galaxies only the inner galaxies are plotted and marked as solid squares (see text). For comparison the $p_{21}/p_{1.5}$ values of sightlines of QSO at $z > 1$ without MgII absorption are plotted in the right hand panel.

where N is the number of surface cells covering the inhomogeneous screen and f_c its covering factor. Using the value of σ_{MgII} estimated at the end of last section, we see that the decrease in $p_{21}/p_{1.5}$ towards lower impact parameters can be explained by the observed increase in $|\text{RM}|$ alone (Figure 2) for $N \sim$ a few. In general, however, the coherence scale of the RM, i.e. N , and f_c might also change as a function of D .

4. DISCUSSION & CONCLUSIONS

The simultaneous increase towards small impact parameters of the RM dispersion on the one hand, and depolarizing effects as probed by $p_{21}/p_{1.5}$, on the other, is consistent with and corroborates previous results (Bernet et al. 2008) suggesting the presence of significant magnetic fields in and around galaxies at distances of several tens of kpc, acting as inhomogeneous Faraday screens (Bernet et al. 2012).

In principle, the observed RM can be attributed to magnetic fields either in the disk or in the halo of the intervening galaxies. The RM associated with the disk magnetic field can be probed using a simple axisymmetric spiral magnetic field model and a distribution of free electrons, n_e , both with radial scalelength and vertical exponential scaleheight of 30kpc and 1.8kpc, respectively (Gómez et al. 2001; Gaensler et al. 2008), and with normalizations, $B_0 = 10\mu\text{G}$, $n_{e0} \sim 0.03\text{cm}^{-3}$, at the galactic center. A simple Monte-Carlo model for the RM from a sample of galaxies at random orientation along the line of sight, then shows that a pure disk magnetic field is not able to account for the observed $|\text{RM}|$ vs D reported in Fig. 2, unless the normalizations or the vertical/radial scales are made unrealistically large. This implies that,

while the disk magnetic field may contribute to the observed RM, other components are most likely present.

It is now established that galactic winds appear in galaxies with star formation rates at low (Bouché et al. 2012), intermediate (Bordoloi et al. 2011; Weiner et al. 2009; Rubin et al. 2010) and high redshifts (Pettini et al. 2002). Bordoloi et al. (2011) finds that MgII absorption in foreground edge-on galaxies at $0.5 < z < 0.9$ shows a strong azimuthal dependence within 50 kpc, indicating the presence of bipolar outflows around the disk rotation axis. Bordoloi et al. (2012) shows that most MgII quasar absorption systems also lie within 45° of the minor axis and at $D < 40$ kpc.

Since our MgII systems show statistically the same properties, the sightlines in our sample will pass through regions above the poles (this will be soon tested with HST imaging of most of the quasar fields in our sample). Further magnetized outflows, although at significantly smaller distances of a few kpc, have also been detected in local galaxies (Haverkorn & Heesen 2012). Therefore, it is likely that the high RM values in Fig. 2 are associated with magnetized outflows.

Can we get meaningful column densities of free electron N_e in the outflows? To calculate N_e we use a simple wind model based on the work of Bouché et al. (2012). We assume that the outflow rate is proportional to the SFR, $\dot{M}_{out} = \eta \text{SFR}$. In addition, for a biconical geometry and constant outflow velocity v_{out} , $\dot{M}_{out} \simeq \frac{\pi}{2} \mu N_g D v_{out} \Theta_{max}$, with N_g the gas column density measured at impact parameter D from a sightline transverse to the outflow, Θ_{max} the opening angle and μ the mean atomic weight (Bouché et al. 2012). For a fully ionized gas, we can then estimate the free electron column density as, $N_e \approx 9 \cdot 10^{19} \text{cm}^{-2} \left(\frac{\eta}{0.5}\right) \left(\frac{\text{SFR}}{10 M_\odot \text{yr}^{-1}}\right) \times \left(\frac{v_{out}}{200 \text{km s}^{-1}}\right)^{-1} \left(\frac{D}{30 \text{kpc}}\right)^{-1} \left(\frac{\Theta_{max}}{30^\circ}\right)^{-1}$, which is essentially the same as the obtained estimate in Bernet et al. (2008) for typical MgII systems, based on HI measurements and an estimate of the ionization correction. This shows that the column density at large D can be substantial in outflows of normal galaxies. Using Eq. 1 and Eq. 2 we then infer a magnetic field strength

$$B_{\parallel} = 54 \mu\text{G} \left(\frac{\sigma_{MgII}}{150 \text{rad m}^{-2}}\right) \left(\frac{s}{10 \text{kpc}}\right) \left(\frac{L}{10 \text{kpc}}\right)^{0.5} \times \left(\frac{f_c}{0.5}\right)^{-0.5} \left(\frac{N_e}{9 \cdot 10^{19} \text{cm}^{-2}}\right)^{-1} \left(\frac{l_c}{3 \text{kpc}}\right)^{-1.5}, \quad (3)$$

where we have set the number of independent RM cells to $N = s^2/l_c^2$, with s the projected linear size of the source at z_{MgII} and have assumed that the scale of the RM fluctuation, l_c , is the same along the sightline and in the plane of the sky. This value of B is higher than the $\sim 10 \mu\text{G}$ obtained in Bernet et al. (2008) because here we consider that the RM screens are inhomogeneous.

This simple analysis shows that magnetized winds can account for the observed $|\text{RM}|$ at large impact parameter reported in Fig. 2. This requires a magnetic field strength B of several tens of μG , which is considerably larger than the few μG fields observed in large scale outflows in nearby galaxies, e.g. NGC5775 (Tüllmann et al. 2000), NGC4666 (Dahlem et al. 1997).

However, fields of such strength are required in

high redshift galaxies by the lack of evolution in the FIR-Radio correlation (Condon 1992; Ivison et al. 2010; Sargent et al. 2010). In fact, the radio emitting electrons would otherwise mostly radiate their energy through inverse Compton scattering on the CMB and/or starlight, both significantly higher at $z \sim 1$ due to cosmological expansion and a $\sim 10\times$ higher SFR, respectively. Since this is not observed, the total magnetic field must have been larger by $\propto \max[\text{SFR}^{1/2}, (1+z)^2] \sim 4$. If this was the case for both large and small scale fields, then values of order of a few tens of μG are found for $z \sim 1$ galaxies, if our reference low- z field is the Galactic one at several μG .

The existence of magnetized outflows in normal galaxies has important implications for α - Ω models of galactic dynamos. Galactic dynamos are thought to be responsible for the origin of large scale magnetic fields in spiral galaxies. However, their efficiency can be severely limited by conservation of magnetic helicity once the small scale magnetic field reaches equipartition with the small scale

kinetic energy of interstellar gas (Vainshtein & Cattaneo 1992; Brandenburg & Subramanian 2005). However, galactic winds can transport magnetic helicity away from the plane of the galaxy and restore the efficiency of α - Ω dynamos, as proposed by Shukurov et al. (2006). Assuming again coexistence of large and small scale fields, our observations support the occurrence of this process and could represent a first observational link between galactic dynamos and magnetized winds at intermediate redshifts.

Understanding the nature of magnetic fields in and around intermediate redshift galaxies deserves further work.

5. ACKNOWLEDGEMENTS

We thank an anonymous referee for his valuable comments. This research has been supported by the Swiss National Science Foundation and made use of observational facilities of the European Southern Observatory (ESO).

REFERENCES

- Bernet, M. L., Miniati, F., & Lilly, S. J. 2010, *ApJ*, 711, 380
 Bernet, M. L., Miniati, F., & Lilly, S. J. 2012, *ApJ*, 761, 144
 Bernet, M. L., Miniati, F., Lilly, S. J., Kronberg, P. P., & Dessauges-Zavadsky, M. 2008, *Nature*, 454, 302
 Bertin, E., & Arnouts, S. 1996, *A&AS*, 117, 393
 Bordoloi, R., Lilly, S. J., Knobel, C., et al. 2011, *ApJ*, 743, 10
 Bordoloi, R., Lilly, S. J., Kacprzak, G. G., & Churchill, C. W. 2012, arXiv:1211.3774
 Bouché, N., Hohensee, W., Vargas, R., et al. 2012, *MNRAS*, 3207
 Brandenburg, A., & Subramanian, K. 2005, *Phys. Rep.*, 417, 1
 Burn, B. J. 1966, *MNRAS*, 133, 67
 Chen, H.-W., Helsby, J. E., Gauthier, J.-R., et al. 2010, *ApJ*, 714, 1521
 Chen, H.-W., & Tinker, J. L. 2008, *ApJ*, 687, 745
 Chen, H.-W., Lanzetta, K. M., Webb, J. K., & Barcons, X. 2001, *ApJ*, 559, 654
 Clarke, T.-E., Kronberg, P., P., Böhringer, H. 2001, *ApJ*, 547, L111
 Coleman, G. D., Wu, C.-C., & Weedman, D. W. 1980, *ApJS*, 43, 393
 Condon, J. J., Cotton, W. D., Greisen, E. W., et al. 1998, *AJ*, 115, 1693
 Condon, J. J. 1992, *ARA&A*, 30, 575
 Dahlem, M., Petr, M. G., Lehnert, M. D., Heckman, T. M., & Ehle, M. 1997, *A&A*, 320, 731
 Feldmann, R., Carollo, C. M., Porciani, C., et al. 2006, *MNRAS*, 372, 565
 Gaensler, B. M., Haverkorn, M., Staveley-Smith, L., et al. 2005, *Science*, 307, 1610
 Gaensler, B. M., Madsen, G. J., Chatterjee, S., & Mao, S. A. 2008, *PASA*, 25, 184
 Gómez, G. C., Benjamin, R. A., & Cox, D. P. 2001, *AJ*, 122, 908
 Han, J. L., Beck, R., & Berkhuijsen, E. M. 1998, *A&A*, 335, 1117
 Haverkorn, M., & Heesen, V. 2012, *Space Sci. Rev.*, 166, 133
 Ivison, R. J., Alexander, D. M., Biggs, A. D., et al. 2010, *MNRAS*, 402, 245
 Jackson, N., Browne, I. W. A., Battye, R. A., Gabuzda, D., & Taylor, A. C. 2010, *MNRAS*, 401, 1388
 Kacprzak, G. G., Churchill, C. W., Steidel, C. C., & Murphy, M. T. 2008, *AJ*, 135, 922
 Kronberg, P. P., Bernet, M. L., Miniati, F., et al. 2008, *ApJ*, 676, 70
 Lanzetta, K. M., Bowen, D. V., Tytler, D., & Webb, J. K. 1995, *ApJ*, 442, 538
 Mao, S. A., Gaensler, B. M., Stanimirović, S., et al. 2008, *ApJ*, 688, 1029
 Murphy, T., Sadler, E. M., Ekers, R. D., et al. 2010, *MNRAS*, 402, 2403
 Oppermann, N., Junklewitz, H., Robbers, G., et al. 2012, *A&A*, 542, A93
 Pettini, M., Rix, S. A., Steidel, C. C., et al. 2002, *Ap&SS*, 281, 461
 Rossetti, A., Dallacasa, D., Fanti, C., Fanti, R., & Mack, K.-H. 2008, *A&A*, 487, 865
 Rubin, K. H. R., Weiner, B. J., Koo, D. C., et al. 2010, *ApJ*, 719, 1503
 Sargent, M. T., Schinnerer, E., Murphy, E., et al. 2010, *ApJS*, 186, 341
 Shukurov, A., Sokoloff, D., Subramanian, K., & Brandenburg, A. 2006, *A&A*, 448, L33
 Taylor, A. R., Stil, J. M., & Sunstrum, C. 2009, *ApJ*, 702, 1230
 Tüllmann, R., Dettmar, R.-J., Soida, M., Urbanik, M., & Rossa, J. 2000, *A&A*, 364, L36
 Vainshtein, S. I., & Cattaneo, F. 1992, *ApJ*, 393, 165
 Weiner, B. J., Coil, A. L., Prochaska, J. X., et al. 2009, *ApJ*, 692, 187

TABLE 1
PROPERTIES OF CANDIDATE HOST GALAXIES

quasar	z_{quasar}	RA (J2000)	Dec (J2000)	z_{MgII}	$W_0(2796)$ (\AA)	ΔRA arcsec	ΔDec arcsec	Ang. sep. arcsec	D kpc	m_g	m_r	m_i	m_z	type	symbol
(1)	(2)	(3)	(4)	(5)	(6)	(7)	(8)	(9)	(10)	(11)	(12)	(13)	(14)	(15)	(16)
4C-02.55	1.043	12:32:00.0	-02:24:05	0.39524	2.03	0.6	-1.9	2.0	10.6	ucl.	□
4C-02.55	0.75689	0.30	1.6	-0.1	1.6	11.8	ucl.	□
MRC0122-003	1.07	01:25:28.8	-00:05:56	0.39943	0.47	-16.8	24.8	30.0	159.9 ^{a)}	ucl.	x
MRC0122-003	0.3971	...	-8.4	-12.1	14.7	76.1 ^{b)}	22.21	20.88	20.52	...	Sbc	x
PKS2326-477	1.299	23:29:17.7	-47:30:19	0.43195	0.38	3.7	-6.8	7.7	43.1	...	21.49	20.92	20.64	Ell	•
PKS2326-477	1.26074	0.66	1.6	5.4	5.6	47.3	...	24.83	24.14	23.80	Sbc	□
4C+06.41	1.270	10:41:17.1	+06:10:17	0.44151	0.69	9.4	2.2	9.7	55.0	22.96	21.14	20.49	...	Ell	□
4C+19.44	0.720	13:57:04.4	+19:19:07	0.45653	0.85	1.6	7.8	7.9	45.8	23.03	21.67	21.17	...	Sbc	•
PKS1244-255	0.633	12:46:46.8	-25:47:49	0.49286	0.68	-3.9	2.3	4.5	27.1	24.47	22.92	22.25	...	Sbc	•
OC-65	0.733	01:41:25.8	-09:28:44	0.50046	0.53	-0.4	-1.4	1.5	9.1	ucl.	•
PKS0130-17	1.022	01:32:43.5	-16:54:49	0.50817	0.59	-3.9	-4.7	6.0	37.1	23.50	22.44	22.14	...	Scd	•
4C+19.34	0.828	10:24:44.8	+19:12:20	0.52766	1.00	-5.6	4.0	6.9	43.2	24.83	23.33	22.84	...	Sbc	○
PKS1615+029	1.339	16:17:49.9	02:46:43	0.52827	0.31	5.7	-2.3	6.2	38.8	24.31	23.01	22.50	...	Sbc	•
4C+01.24	1.024	09:09:10.1	+01:21:36	0.53587	0.44	-6.8	0.9	7.0	44.1	23.06	21.71	21.26	...	Sbc	•
PKSB1419-272	0.985	14:22:49.2	-27:27:56	0.55821	0.44	11.2	8.0	13.7	88.6	23.36	21.85	20.91	...	Ell	•
OX+57	1.932	21:36:38.6	+00:41:54	0.62855	0.60	5.6	-0.3	5.6	38.1	ucl.	•
OX-192	0.672	21:58:06.3	-15:01:09	0.63205	1.40	2.8	1.6	3.2	21.8	24.33	22.68	21.39	...	Ell	•
PKS0420-01	0.915	04:23:15.8	-01:20:33	0.63291	0.77	5.7	-13.3	13.5	92.5	24.09	22.45	21.68	...	Ell	•
3C208	1.112	08:53:08.6	+13:52:55	0.65262	0.62	0.3	-6.6	6.6	45.5	...	21.90	20.70	20.34	Ell	□
3C208	0.93537	0.40	-3.5	6.7	7.6	60.4	...	23.07	22.40	22.09	Scd	□
PKS0038-020	1.178	00:40:57.6	-01:46:32	0.68271	0.35	-10.8	-3.8	11.5	78.2	23.82	22.88	22.26	...	Scd	○
PKS2204-54	1.206	22:07:43.7	-53:46:34	0.6877	0.73	-9.7	-5.3	11.1	78.7	23.35	22.40	22.10	...	Scd	○
PKS0839+18	1.270	08:42:05.1	+18:35:41	0.71118	0.56	-5.4	5.4	7.6	54.7	22.70	21.71	21.14	...	Scd	•
4C+13.46	1.139	12:13:32.1	13:07:21	0.77189	1.29	-0.6	1.8	1.9	14.1	ucl.	○
4C+6.69	0.99	21:48:05.4	+06:57:39	0.79086	0.55	0.3	-5.8	5.8	43.4	23.82	22.74	22.15	...	Scd	•
PKS0402-362	1.417	04:03:53.7	-36:05:02	0.79688	1.80	1.8	2.5	3.1	23.2	23.28	22.61	21.83	...	Scd	•
PKS2223-05	1.404	22:25:47.2	-04:57:01	0.84652	0.60	-2.1	6.7	7.0	53.9	...	23.47	22.26	21.49	Ell	•
PKS0506-61	1.093	05:06:43.9	-61:09:41	0.92269	0.49	1.8	4.0	4.4	34.6	...	23.42	22.64	22.33	Scd	○
PKS0112-017	1.365	01:15:17.1	-01:27:05	1.18965	0.90	2.0	-2.6	3.3	27.4	ucl.	•
PKS0332-403	1.445	03:34:13.7	-40:08:25	1.20898	0.79	3.4	10.3	10.9	91.0	...	23.66	22.66	21.74	Ell	x
PKS0332-403	1.445	03:34:13.7	-40:08:25	0.8	...	-3.4	3.3	4.8	36.1 ^{c)}	...	23.31	21.93	21.43	Ell	x
PKS1143-245	1.940	11:46:08.1	-24:47:33	1.24514	0.30	10.0	0.3	10.0	84.0	...	23.70	23.19	22.53	Sbc	□
PKS1143-245	1.52066	0.46	2.2	-1.7	2.8	23.9	ucl.	□
OQ135	1.612	14:23:30.1	+11:59:51	1.36063	0.51	-12.9	-3.1	13.3	112.8	...	23.62	22.87	22.12	Sbc	•
quasar fields with alternative candidate galaxies															
PKS0130-17	1.022	01:32:43.5	-16:54:49	0.50817	0.59	11.8	6.0	13.2	81.0	22.61	21.76	21.42	...	Sbc	...
4C+19.34	0.828	10:24:44.8	+19:12:20	0.52766	1.00	2.2	-3.4	4.0	25.0	ucl.	...
PKS1615+029	1.339	16:17:49.9	02:46:43	0.52827	0.31	3.9	4.8	6.2	38.8	22.66	21.19	20.43	...	Ell	...
4C+01.24	1.024	09:09:10.1	+01:21:36	0.53587	0.44	11.7	10.3	15.5	97.8	24.16	22.53	21.80	...	Ell	...
PKS0038-020	1.178	00:40:57.6	-01:46:32	0.68271	0.35	13.2	8.3	15.6	110.3	23.43	22.64	22.06	...	Scd	...
PKS2204-54	1.206	22:07:43.7	-53:46:34	0.6877	0.73	3.5	-7.4	8.2	58.1	24.12	24.04	23.56	...	Irr	...
PKS0839+18	1.270	08:42:05.1	+18:35:41	0.71118	0.56	-3.3	7.5	8.1	58.2	24.03	22.64	21.91	...	Sbc	...
4C+13.46	1.139	12:13:32.1	13:07:21	0.77189	1.29	3.1	0.4	3.1	23.0	24.13	22.30	21.14	...	Ell	...
PKS0506-61	1.093	05:06:43.9	-61:09:41	0.92269	0.49	-7.6	-1.4	7.7	60.6	...	23.08	22.39	22.07	Scd	...
PKS1143-245	1.940	11:46:08.1	-24:47:33	1.52066	0.46	-9.1	-3.6	9.7	82.9	...	23.61	23.42	22.79	Scd	...